Maturilli *et al. Earth, Planets and Space* (2016) 68:113
DOI 10.1186/s40623-016-0489-y

Earth, Planets and Space

LETTER

Open Access

Characterization of asteroid analogues by means of emission and reflectance spectroscopy in the 1- to 100-μm spectral range

Alessandro Maturilli[1*], Jörn Helbert[1], Sabrina Ferrari[1], Björn Davidsson[2] and Mario D'Amore[1]

Abstract

The last decades have seen a large number of missions targeting small bodies in the solar system. NASA, ESA and JAXA sent missions to different solar system small bodies (SSSB), and the Japan mission Hayabusa returned samples from the surface of the S-type asteroid Itokawa. JAXA launched in 2014 a follow-up mission (Hayabusa2) to collect a sample from carbonaceous (C-type) asteroid 1999 JU3 asteroid and bring it back to Earth. The NASA's OSIRIS-REx mission will launch in September 2016 to explore the carbonaceous asteroid Bennu. Despite an already existing rich collection of reflectance and emissivity spectral libraries for asteroid analogues, those are mostly based on measurements in air for a spectral range covering the visible to the medium infrared (approximately, from 0.4 to 25 μm). To characterize minerals, rocks and meteorites suitable for being surface analogues for asteroids and SSSB in general, spectroscopic measurements are needed for a wider spectral range and in vacuum, conditions that more closely resemble those found on asteroid surfaces. To fill this gap we acquired spectral measurements over a large spectral range (1–100 μm) for several meteorites and other analogues at the Planetary Emissivity Laboratory of the German Aerospace Center in Berlin. Those data provide more direct analogues for asteroid surfaces and expand our existing database of emissivity and reflectance measurements.

Keywords: Asteroid analogue materials, Emissivity measurements, Reflectance measurements, Infrared spectroscopy

Introduction

Solar system small bodies (SSSB) are remnants of the process that led to the formation of the solar system from the solar nebula. Information on their composition and physical properties is a key to understand the formation and evolution of our solar system. Asteroids and comets may contain the molecular precursors (organic molecules such as amino acids) to the origin of life on Earth and could possibly be the source of water that formed the Earth's oceans.

When electromagnetic radiation of a specified range of wavelengths passes through matter, energy is absorbed at some of the wavelengths and not others, by a variety of processes. By observing which wavelengths a molecular species absorbs, and to what extent it absorbs them, we can gain information about the nature of the electronic, vibrational and rotational transitions that a molecule is able to undergo and thus information about its structure. The infrared region of the electromagnetic spectrum, for instance, contains energies corresponding to the vibrational frequencies of bonds in organic molecules (stretching and bending) (Farmer 1974).

The near-infrared (NIR) region from 1 to 5 μm contains primarily information on overtones and combinations for phyllosilicates, most sorosilicates, hydroxides, some sulfates, amphiboles, carbonates, soil water and organic matter; the thermal-infrared (TIR) region from 5 to 100 μm contains mostly information on Si–O lattice vibrations for silicates (quartz, feldspars, clay), other than mafic, carbonate mineral group and organic compounds (Chabrillat et al. 2013).

To fully understand the mineralogical composition of SSSB and the implications to solar system formation

*Correspondence: alessandro.maturilli@dlr.de
[1] Institute of Planetary Research, German Aerospace Center DLR, Rutherfordstr. 2, 12489 Berlin, Germany
Full list of author information is available at the end of the article

and the nature of water in the universe, it is important to investigate and integrate data over the whole spectral range from 1 to 100 μm.

In the last years, Earth- and space-based spectroscopic infrared observations have helped to constrain the chemical and mineralogical composition of several small bodies.

During its cruise to the comet 67P/Churyumov–Gerasimenko (Heinemann et al. 2013), the ESA Rosetta spacecraft performed flybys of asteroid 21 Lutetia and 2867 Steins (Glassmeier et al. 2007). Vernazza et al. (2011) show spectral similarities of Lutetia to E chondrites in the Vis–NIR spectral range. Combining together the information available from ground observations, space observations and Rosetta data, Barucci et al. (2012) concluded that spectral variations on Lutetia's surface are explained by different surface compositions and textures. Furthermore, Lutetia differs from all asteroids visited from spacecraft missions, as well as asteroids observed from ground. Its surface is composed of materials similar to chondrites: Some southern regions are similar to carbonaceous chondrites (like CV, CO, CK), while the northern hemisphere shows more similarity to a mixture of enstatite and carbonaceous chondrites.

Rosetta's flyby of Steins was too short and distant to get enough data to understand its surface composition. Telescopic observations with the infrared spectrograph (IRS) of the Spitzer Space Telescope concluded that Steins emissivity spectrum is similar to the enstatite achondrite meteorites and to the mineral enstatite, confirming the rare E-type classification already suggested on the basis of ground-based spectral and polarimetric observations (Barucci et al. 2008).

The NASA Dawn mission, launched in 2007 to study two proto-planets of the asteroid belt Vesta and Ceres (Russell et al. 2007), is currently in orbit around the dwarf planet Ceres.

Ceres is a very complicated object, which experienced complex internal chemistry processes that may have extended to the surface. Spectral observations identified hydrated phases (clays, silicates, salts) leading to a possible comparison with water-rich carbonaceous chondrite material (McCord and Sotin 2005, Rivkin et al. 2011).

Vesta (a volatile-depleted body), largely recognized as the source of the howardite–eucrite–diogenite (HED) meteorites, thought to be the result of collisions of several proto-planet bodies with Vesta (Burbine et al. 2001). A weak hydration signature at 3 μm was detected from telescopic observations (Rivkin et al. 2006; Hasegawa et al. 2003), but not confirmed by later observations. The VIR imaging spectrometer on Dawn detected OH (hydroxyl) bands on regions of Vesta's surface (De Sanctis et al. 2012). The distribution of the hydration band on Vesta is likely related to differences in the mineralogy of its surface materials and/or the presence of exogenous OH-bearing materials. The analysis of samples returned by the Hayabusa spacecraft has confirmed the LL chondrite composition of Itokawa (Nakamura et al. 2011), with the identification of olivine and pyroxene as major components, followed by plagioclases. Carbonaceous materials among the particles collected by the Hayabusa spacecraft sample catcher are discussed in Uesugi et al. (2014) and Kitajima et al. (2015).

A new light on surface composition of SSSB will come from two future missions. JAXA launched in 2014 the Hayabusa2 mission to collect a sample from a C-type asteroid 1999 JU3 and bring it back to Earth (Saiki et al. 2013). This class of asteroids is thought to contain more organics and water, linking them closely to the origin and distribution of volatiles (see also King et al. 2015). The mission features a near-infrared spectrometer (Iwata et al. 2014), a mid-infrared imager (Okada et al. 2012) and a radiometer with four narrow-band spectral channels on the lander (Grott et al. 2013).

The NASA's OSIRIS-REx mission is scheduled for launch in 2016 to explore the carbonaceous asteroid Bennu (Lauretta et al. 2015). At least 60 grams of pristine surface will be collected and brought back to Earth. Visible and near-infrared spectrometer (Simon-Miller and Reuter 2013) and a thermal-infrared spectrometer (Hamilton and Christensen 2014) operate on the spacecraft. Instrument specifications for both missions are listed in Table 1.

Several previous studies have been devoted to building databases of VNIR (visible near infrared)-TIR spectra of meteorites and analogues. Among them, Salisbury et al. (1991) measured reflectance (mostly bi-conical) spectra in air of many meteorites in the 2.5- to 13-μm spectral range. Emissivity (in air) spectra for large grain size samples (710–1000 μm) in the 5- to 45-μm spectral range were reported by Christensen et al. (2000). Moroz et al. (2006) concentrated on hydration features of some meteorites, acquiring bi-conical reflectance between 2.5 and 14 μm. The ASTER spectral library (Baldridge et al. 2009) contains hemispherical reflectance of natural and man-made materials measured in air in the 0.4- to 15-μm spectral range. The USGS spectral library described in Clark et al. (2007) contains reflectance measurements in dry-nitrogen atmosphere for the spectral range 0.2–25 μm (and often extended to 150 μm). The NASA RELAB database contains reflectance spectra of meteorites in the 0.3- to 2.5-μm spectral range (Gaffey 1976). Cloutis and colleagues (cf. Cloutis et al. 2013 and references therein) collected reflectance spectra of meteorites in the spectral range from 0.3 to 2.5 μm. Maturilli et al. (2008) and Maturilli and Helbert (2014) measured emissivity of

Table 1 Details on instruments flying to next asteroid-targeted missions

Name/mission	Instrument type	Resolving power (*R*) Spectral resolution	Spatial resolution	Spectral range (μm)	SNR
OVIRS/OSIRIS-REX	Grating point	$R = 125–350$	20 m global 0.08–2 m target	0.4–4.3	NA
OTES/OSIRIS-REX	FTIR point	10 cm^{-1}	4 m	4–50	>325 in 7–33 μm
TIR imager Hayabusa2	TIR imager	Broadband imager	10 m	8–12	NETD < 0.5 K
NIRS3/Hayabusa2	Grating point	20 nm	40 m	1.8–3.2	>50
MARA/Hayabusa2	4 narrow filters and 2 broad filter	2–4 μm	20 cm	5.5–7, 8–9.5, 9.5–11.5, and 13.5–15.5	NETD < 0.1 K

minerals and rocks for several grain size ranges in purged air between 2.5 and 50 μm. Morlok et al. (2010, 2012) measured mid-infrared (5–25 μm) transmission/absorption spectra of meteorites. This list is not complete but features a representative selection of the typical spectral libraries that are available for the interpretation of remote sensing infrared measurements of asteroid surface. Despite the high scientific value of existing spectral libraries, for the most direct comparison with radiation emitted from an airless SSSB a spectral database of emissivity measurements acquired with a high signal-to-noise ratio in vacuum over a large spectral range and for small grain sizes is needed.

At PEL we conducted spectroscopic measurements of several meteorites and other analogues for asteroid surfaces. Here we present emissivity and reflectance of seven fine-powdered surface analogues, which were measured under vacuum in the 1- to 100-μm spectral range. These data form an important set of asteroid analogues that will directly support the data analysis of ongoing and future missions. It can also help to plan future missions and provides important input for thermal models of small bodies (cf. Davidsson et al. 2015).

Methods

Instrument description

Two spectrometers at PEL are equipped with external chambers to measure emissivity. The Bruker Vertex 80 V FTIR spectrometer is operated under medium vacuum (~0.7 mbar, 70 Pa) to remove atmospheric features from the spectra. The 1- to 16-μm spectral range is covered by using a nitrogen-cooled MCT (mercury cadmium telluride) detector and KBr beamsplitter. The 16- to 100-μm spectral range is acquired with a room-temperature DTGS (deuterated triglycine sulfate) detector and Mylar multilayer beamsplitter. Standard spectral resolution used is 4 cm^{-1}, and spot size is 2 mm for reflectance and 49 mm for emissivity measurements. A Bruker A513 accessory is used for bi-conical reflectance measurements (Maturilli et al. 2014). The viewing cone of the A513 has an aperture of 17°, not small enough to define our measurements as bi-directional. Gold-coated sandpaper is used as reference standard for reflectance measurements along the entire 1- to 100-μm spectral range.

The Bruker IFS88 FTIR spectrometer with its attached emissivity chamber is used for emissivity measurements in a purging environment (Maturilli et al. 2006, 2008; Maturilli and Helbert 2014).

The spectral range 1–16 μm is covered with a nitrogen-cooled MCT detector + KBr beamsplitter (Maturilli et al. 2006, 2008). Standard spectral resolution used is of 4 cm^{-1}, and spot size is 24 mm for emissivity measurements.

It is well known that only hemispherical reflectance measurements can be directly compared with emissivity measurement of samples under thermal equilibrium with the surrounding medium (Salisbury and Walter 1989). Therefore, strictly speaking our bi-conical reflectance measurements (with angles incidence = emission = 13°, no correction for grazing angles needed) can only qualitatively be compared to our emissivity measurements made under vacuum (where the lack of air between the grains gives rise to vertical thermal gradients). However, bi-conical reflectance measurements are more representative of the way spacecraft instruments obtain reflectance measurements than hemispherical reflectance measurements. Therefore, data obtained by combining bi-conical reflectance and emission measurements can be applied directly to the analysis of data returned by NIR/TIR instruments.

Sample preparation and data acquisition

An external chamber is used to measure emissivity under vacuum. Each sample is poured in a stainless steel cup to a 3-mm-thick uniform layer; the cup is placed on an induction pancake coil. Induction heating is used to heat up the cup and thereby the samples contained. By using the induction properties to heat the cups, we do not set the heater temperature, but the intensity of the current that we send to the induction coil. The whole cup (made

of steel) is heated uniformly by the induction process; therefore, our samples are heated from below as well as from the side (rims) of the cup and are not heated/illuminated from above. A thermopile temperature sensor (whose head is a long, thin wire of 0.2 mm) is put in contact with the emitting surface, to read the sample temperature. Blast furnace slag, poured in a stainless steel cup and under exactly the same geometric configuration as the samples, is heated to sample temperature and is used as calibration blackbody. The calibrated sample emissivity is then calculated by dividing the sample radiance to the blackbody radiance (measured at the same temperature) and then multiplying this resulting spectrum for the emissivity spectrum of the blackbody material. The emissivity curve of the slag has been retrieved by measuring the blast furnace slag vs. a commercial blackbody, painted with a black and well-characterized coating (Acktar Fractal Black). For each spectrum (in emission or reflectance) 500 repeated scans are measured to improve the signal-to-noise ratio; the acquisition procedure takes 4 min for emission and 7 min for reflectance. Further details on instrumental setup and calibration procedures can be found in Helbert et al. (2013) and references therein. Emissivity measurements under purged air are performed using the same cups, reference body and methodology used for vacuum measurements, with the only difference being the use of a traditional heating resistor to heat the samples from below.

Sample selection

We measured the emissivity (in vacuum and purged air) and reflectance spectra (in vacuum) for a group of relevant analogues of interest for the upcoming and ongoing asteroid missions. To measure emissivity in our sample cups we need at least 3–4 g of powdered materials. This demand had a strong influence on the chosen samples, forcing us to consider in this study only meteorites we had in abundant quantity. The suite consists of seven samples: three meteorites and four terrestrial analogue materials. Meteorite Allende represents the CV group of the carbonaceous chondrites meteorites (Scott et al. 1988; Brearley 1996; Bland et al. 2003), displaying good spectral matches with asteroid Lutetia (Barucci et al. 2008; Vernazza et al. 2011). Bland et al. (2004) analyzed Allende meteorite by X-ray diffraction (XRD) and suggested the following composition (wt %): olivine (81.6 %), enstatite (5.9 %), plagioclase (0.9 %), magnetite (0.3 %), Fe–Ni metal (0.2 %) and pentlandite (iron–nickel sulfide, 11.1 %). Because of the Allende's un-equilibrated condition (relatively unaltered meteorite), olivines cover the entire solid solution range in terms of Mg vs. Fe content. Murchison meteorite accounts for the CM group (Fuchs et al. 1973) which typically shows traces of alteration by water-rich fluids on its parent body. XRD analysis of Murchison (Bland et al. 2004) suggests a high amount of matrix, mainly constituted by cronstedtite and tochilinite (58.5 wt%), followed by serpentine (22.8 %), olivine (Fo50–100, 11.6 %), enstatite (2.2 %), pyrrhotite (2.9 %) and minor amounts of pentlandite, magnetite and calcite. Meteorite Millbillillie is an achondritic eucrite, possibly originating from asteroid Vesta (Hiroi et al. 1995). XRD analysis reported by Cloutis et al. (2013) indicates the following phase abundances: plagioclase (49 wt%), pigeonite (24 %), augite (12 %), orthopyroxene (14 %) and minor amounts of ilmenite, chromite and troilite.

In addition to meteorites, four terrestrial samples belonging to the PEL-DLR collection have been chosen as asteroid analogues. X-ray fluorescence analyses conducted at GeoForschungsZentrum (GFZ) in Potsdam, Berlin (Germany), provide chemical data (see Additional file 1: Table S1). X-ray powder diffraction (XRD) analyses have been conducted at PEL using a portable inXitu Terra X-ray diffraction instrument to assess the presence of additional phases that may be significant for the spectroscopic measurements. Analytic method and data are available in the Additional file 2; results are included in the following description. A terrestrial enstatite from Ødegården, Bamble (Norway, Iijima and Buseck 1975), which presents no additional phases (ref. Additional file 2 for XRD pattern) other than few percent of talc that is not enough to rise spectral features, is chosen to represent E-type asteroids (Zellner et al. 1977) such as Steins. A sample of natural commercial graphite from Kropfmühl AG (Germany) has been included because graphite (igneous or as aggregates) has been detected in most enstatite chondrites (Rubin 1997). Montmorillonite supplied by Iko-Erbslöh company (Germany) and serpentine (lizardite and clinochrysotile, with brucite) from Snarum (Norway) complete the set of analogue materials, representing phyllosilicates formed on the asteroidal surfaces by aqueous alteration processes of the original rocky asteroidal parent body materials (Vilas and Gaffey 1989).

For this study we measured grain size separate < 25 μm, the finer particles being a reasonable analogue of asteroidal regolith in terms of particle size, as suggested from Salisbury et al. (1991) and Pieters et al. (1993). For emissivity measurements under vacuum and under purging we kept the sample temperature as low as possible (100 °C on the surface) while still having a good signal-to-noise ratio.

Results and discussion

Figures 1, 2, 3, 4, 5, 6 and 7 show the spectral measurements for the asteroid analogue materials we selected for our sample set. For each figure we split the spectra in 2 panels, for a better visualization of the data. In the left panel

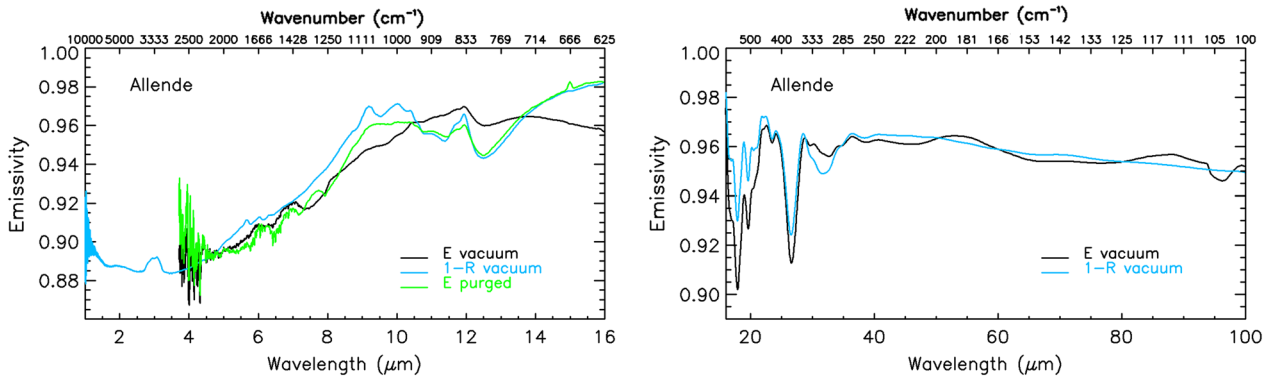

Fig. 1 Emissivity and reflectance measurements for meteorite Allende; *left panel* shows emissivity in vacuum and under purging, compared with 1-R in the NIR-MIR; *right panel* shows emissivity in vacuum compared with 1-R in the TIR

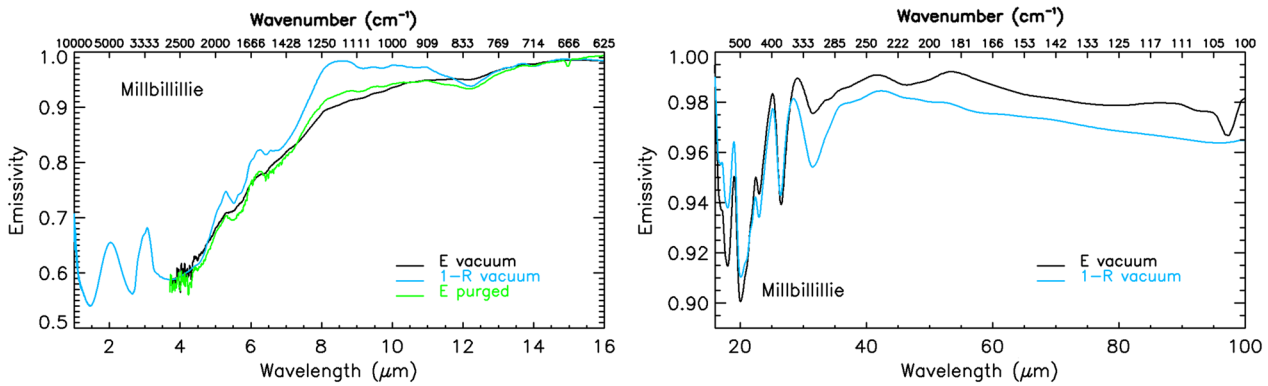

Fig. 2 Emissivity and reflectance measurements for meteorite Millbillillie; *left panel* shows emissivity in vacuum and under purging, compared with 1-R in the NIR-MIR; *right panel* shows emissivity in vacuum compared with 1-R in the TIR

we show emissivity measured in vacuum and under purging and 1-reflectance measured under vacuum in the NIR and MIR (medium infrared) spectral range (1–16 μm). In the right panel we show emissivity and 1-reflectance measured in vacuum in the thermal-infrared (TIR) spectral range (16–100 μm). An additional upper X-axis reports wave numbers (cm^{-1}) to facilitate the plot comprehension. In a recent paper we show that bi-conical reflectance spectra of samples measured at PEL under purging or under vacuum conditions are identical (Maturilli et al. 2015), but the measurements under vacuum are preferable because they are free of atmospheric spectral features.

Emissivity and 1-R (R is bi-conical reflectance) show systematic differences under vacuum, which is already extensively discussed in the literature (cf. Salisbury et al. 1994). However, it is important to note that in a powdered sample heated in vacuum, vertical thermal gradients develop and are mostly influenced from the intensity of vacuum, and from the material thermal conductivity, that is very strongly controlled by particle size because of its effect on porosity (Salisbury et al. 1994). Also, it is not surprising that our 1-R spectra are much similar to emissivity measurements taken under purging environment (where the sample temperature is vertically homogeneous, and also the Kirchhoff's law is valid) and differ significantly from emissivity measurements taken under vacuum (where thermal gradients arise in the sample), as already pointed out in Salisbury et al. (1994). The vacuum intensity in our external chamber is "medium" (typical values between 30 and 0.001 mbar) and is not fully comparable with the high vacuum of outer space. Therefore, only from the point of view of vacuum, we expect higher thermal gradients on asteroid surface than in our sample cups. On the other hand we chose the smallest standard grain size range used at PEL (<25 μm). Previous studies (e.g., Logan et al. 1973) show that most of the particles in this range fall below the 2-μm grain size range, which results in an increase of the vertical temperature gradient in the sample, because the sample porosity is one of the key factors driving the intensity of thermal gradient. We

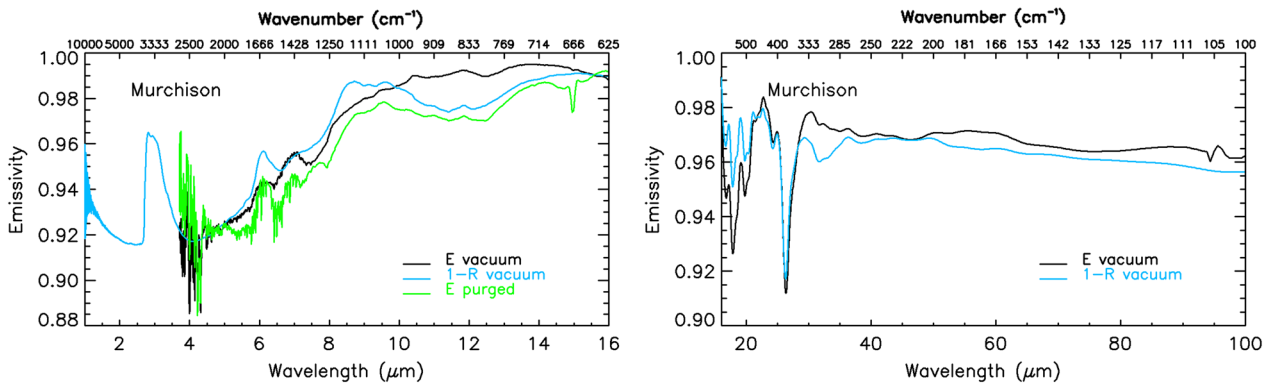

Fig. 3 Emissivity and reflectance measurements for meteorite Murchison; *left panel* shows emissivity in vacuum and under purging, compared with 1-R in the NIR-MIR; *right panel* shows emissivity in vacuum compared with 1-R in the TIR

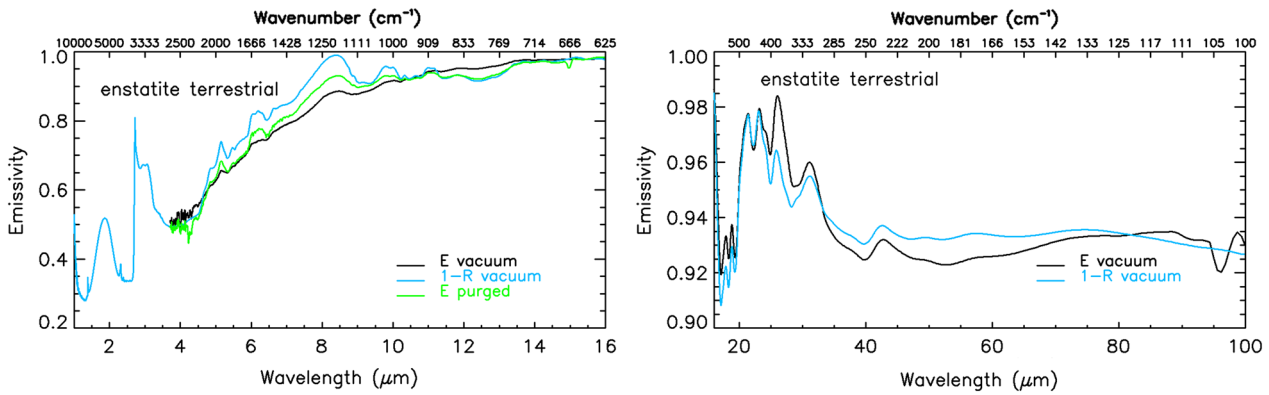

Fig. 4 Emissivity and reflectance measurements for terrestrial enstatite; *left panel* shows emissivity in vacuum and under purging, compared with 1-R in the NIR-MIR; *right panel* shows emissivity in vacuum compared with 1-R in the TIR

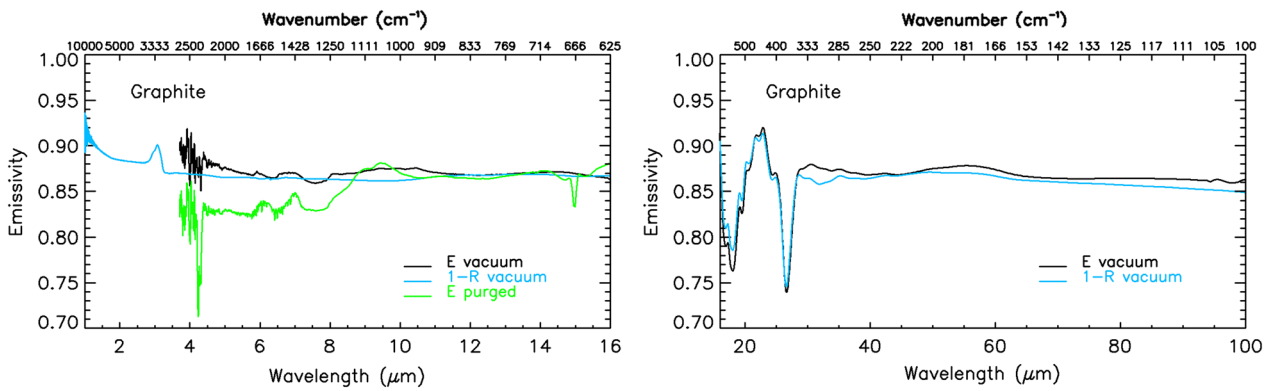

Fig. 5 Emissivity and reflectance measurements for graphite; *left panel* shows emissivity in vacuum and under purging, compared with 1-R in the NIR-MIR; *right panel* shows emissivity in vacuum compared with 1-R in the TIR

can therefore conclude that our instrumental setup and sample selection are reasonably good approximations reproducing asteroid surficial emissivity spectra.

We discard data below 4 μm because of too low signal-to-noise ratio, due to the low temperature used to heat the samples in this experiment. In the spectra measured

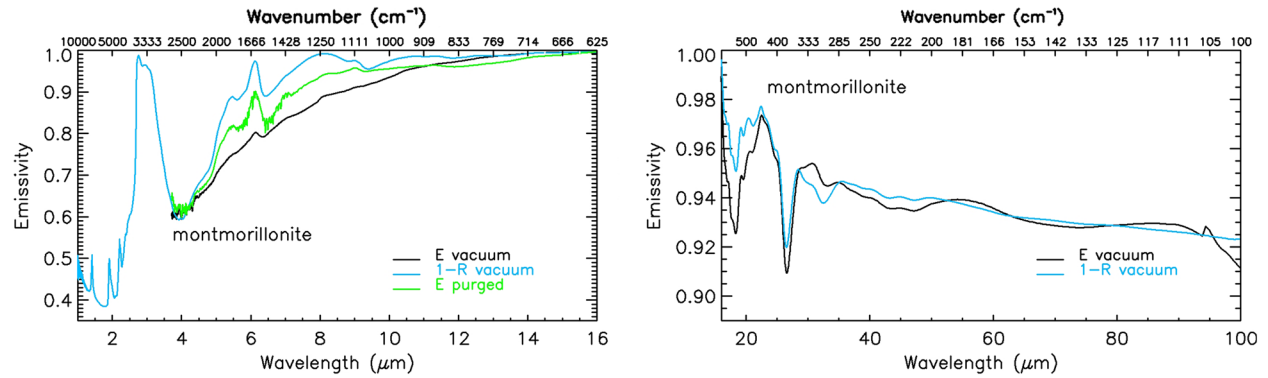

Fig. 6 Emissivity and reflectance measurements for montmorillonite; *left panel* shows emissivity in vacuum and under purging, compared with 1-R in the NIR-MIR; *right panel* shows emissivity in vacuum compared with 1-R in the TIR

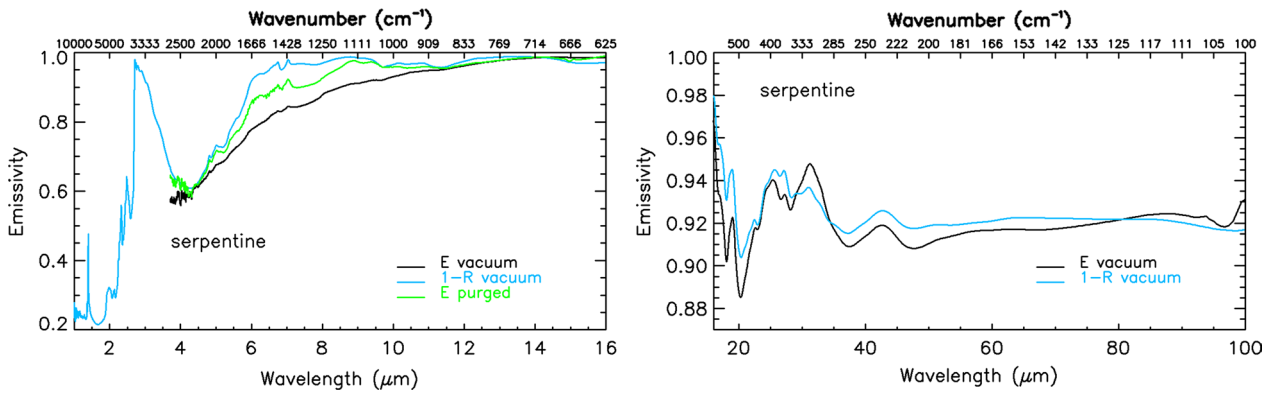

Fig. 7 Emissivity and reflectance measurements for serpentine; *left panel* shows emissivity in vacuum and under purging, compared with 1-R in the NIR-MIR; *right panel* shows emissivity in vacuum compared with 1-R in the TIR

under purging some features of atmospheric gas absorption (cf. CO_2 band at 15 μm) are still present, due to slight imperfections in the air purging mechanism.

Carbonaceous chondrites display large chondrules of Mg-rich olivine, which provides the most prominent bands of the Allende sample spectra (Fig. 1). The lack of well-shaped O–H stretching vibration bands between 2 and 3 μm suggests a low-grade alteration of the sample (Salisbury and Hunt 1974; Miyamoto 1988). Lack of H–O–H bending vibration at 6.1 micron in the spectra under vacuum precludes the presence of surface adsorbed water in the sample. Most of the vibrational bands observable between 8 and 16 μm appear strongly reduced in the vacuum emissivity spectrum with respect to the purged emissivity, due to thermal gradients in the sample (Logan and Hunt 1970) and to the weakening (disappearance in high vacuum) of the transparency feature in vacuum (Salisbury et al. 1991). On the other hand some overtones below 7 μm are more prominent with respect to the other spectra shown in Fig. 1. The deep emissivity minimum (comparable to the transparency feature of olivine) at 12.5 μm suggests a dominant surface scattering and confirms the fine grain size of the sample (Salisbury and Walter 1989; Mustard and Hays 1997).

Millbillillie meteorite spectra (Fig. 2) confirm the small grain size range of the sample by the enhanced transparency feature around 12.4 μm. The Christiansen feature (CF) broadens due to the combination of different silicates as both Ca-rich pyroxene and plagioclase are present, whereas the weak Reststrahlen bands below 16 μm appear obliterated in the vacuum emissivity spectrum, as already shown in Salisbury et al. (1991). Spectra of achondrites such as Millbillillie show strong bands at 19.8 μm and 23.9 μm that can be due to orthopyroxene and Ca-rich pyroxene (Morlok et al. 2012). Similar results arise from the Murchison meteorite spectra in Fig. 3. The broadness and lack of structure of the 10-μm features in the spectra of Murchison may result from the overlapping of Si–O absorptions of various phyllosilicates composing the matrices of CM chondrites (Moroz et al.

2006). The vacuum emissivity spectrum of Murchison reveals the weak emissivity maximum (reflectance minimum) near 10.5 μm that is typical of olivine. Another confirmation of olivine content in Murchison is found with the strong band at 19.6 μm (Morlok et al. 2010). The band at 22.5 micron is typical for serpentine phyllosilicate, while the band at 27 μm can be found in graphite and montmorillonite.

Typical phyllosilicates band around 9.5–10 μm, well shaped both in montmorillonite and in serpentine spectra (Figs. 6, 7), appears strongly suppressed in Murchison measurements, whereas bands around 3 and 6.5 μm, characteristic of hydrated phases (Morlok et al. 2010), are still prominent.

Low-Ca Mg-rich orthopyroxenes are the main constituent of E-type asteroids and—in combination with olivine and iron–nickel metals—of ordinary chondrites. Spectra of a natural sample of enstatite (Fig. 4) display a distinct CF at 8.4 μm and a broad Reststrahlen band around 9.3 μm (Salisbury et al. 1991) as well as an additional broad Reststrahlen feature between 12 and 14 μm (that is shifted to longer wavelengths in the spectra of high-Ca pyroxenes). The characteristic 18-μm band (Barucci et al. 2008) is detectable in our enstatite sample. In the emissivity spectrum of our enstatite sample we can recognize a distinctive band around 39 μm together with a very broad feature above 43 μm centered around 53 μm. The enstatite band around 97 μm (a similar band is present in the serpentine spectrum too) can be seen in both our Allende and Millbillillie meteorites.

Thanks to the variability of techniques and wavelength extension of our measurements, for each of the samples in our dataset it is possible to concurrently recognize multiple features previously described in literature by other authors. The set of spectral measurements for asteroid analogues we are presenting can also help in the planning of future missions and provides important input for thermal models of small bodies (cf. Davidsson et al. 2015). Specifically, such models solve the heat conduction equation in order to estimate the temperature in the regolith as function of time and depth below the surface. The upper boundary condition of this equation contains a term for thermal radiative heat loss to space that depends on the surface temperature and the integrated hemispherical emissivity E. The latter parameter is the ratio between the energy loss at all wavelengths of an actual surface to that of an ideal blackbody at the same temperature. In thermophysical modeling it is not uncommon that this parameter is set to unity or 0.9, for lack of better alternatives. The current measurements offer the possibility to calculate E for specific minerals and temperature intervals for application in thermophysical models. This is important for minerals such as enstatite and phyllosilicates, which have low emissivity at wavelengths below 8 μm. Failure of a model to account for this property will result in incorrect surface temperatures, particularly when surfaces are being heated above 350 K (80 °C).

Conclusions

The growing number of sophisticated missions to small bodies in the solar system requires dedicated laboratory work to maximize the science return of remote sensing observations and support sampling site selection.

The set of analogues presented here is a first step toward this goal. It provides high signal-to-noise spectra for a range of potential surface materials obtained with a wide spectral coverage encompassing all currently flying and planned NIR and TIR instruments. Already this small starting set allows a number of interesting conclusions.

The compositional information that can be obtained in the TIR (especially if we start around 5 microns) is highly complementary to the NIR. On the other hand most (but not all) of the spectral information is contained in the wavelength range <30 microns. Only very few analogues show spectral features between 30 and 100 microns, and they all have a very low spectral contrast. This is interesting for trade-offs concerning instrument design. In general, it seems that spectral coverage beyond 50 microns does not justify massive increases in the complexity (and therefore cost and mass) for a TIR instrument. Nevertheless, if the spectrometer target has areas that experience polar night, they will be very cold and will only emit radiation at very long wavelengths. If these can be measured, it provides important information about, e.g., thermal inertia at large depths. This was done for comet 67P (Biver et al. 2015) that had temperatures of 30 K in the polar night region. The radiation was being observed at cm wavelengths with the MIRO instruments (that was the only instrument available that could cover this longer wavelengths region), though a spectrometer covering the 100-micron region would have been optimal.

As expected, the small grain sizes used in this study result in very low spectral contrast. However, it is clear from the spectra shown here that even the low spectral contrast of a very fine-grained regolith would be enough to identify major phases. Given that Itokawa actually showed a much coarser grain size distribution (particle size ranges between 30 and 180 μm, Tsuchiyama et al. 2011), it is clear that mid-infrared observations are a highly diagnostic tool for the study of the surface of asteroids. The most likely thermal inertia for 1999JU3 ranges between 200 and 600 J m^{-2} $s^{-0.5}$ K^{-1}, about a factor of 2 lower than the value for 25143 Itokawa (Mueller et al. 2010). This indicates that the surface lies somewhere between a thick-dust regolith and a rock/boulder/

cm-sized, gravel-dominated surface like that of 25143 Itokawa. Based on the obtained laboratory results TIR instruments would also make a valuable addition for future missions to targets with very fine-grained surfaces.

Furthermore, our spectral measurements allow to accurately estimate the emissivity for specific minerals, which can be used for application in thermophysical models.

Additional files

Additional file 1. XRF analysis of the terrestrial analogues used in this study.

Additional file 2. XRF pattern for terrestrial enstatite (Norway) described in this study.

Abbreviations

ESA: European Space Agency; NASA: National Aeronautics and Space Administration; JAXA: Japan Aerospace Exploration Agency; SSSB: solar system small bodies; MASCOT: Mobile Asteroid Surface Scout; OSIRIS-REx: Origins, Spectral Interpretation, Resource Identification, Security, Regolith Explorer; PEL: Planetary Emissivity Laboratory; DLR: Deutsche Zentrum für Luft- und Raumfahrt e. V (German Aerospace Agency); VIR: visible infrared spectrometer; HED: howardite–eucrite–diogenite; MARA: MASCOT Radiometer; OTES: OSIRIS-REx Thermal Emission Spectrometer; THERMAP: thermal mapper; FTIR: Fourier transform infrared; NIR: near infrared; MIR: medium infrared; TIR: thermal infrared; MCT: mercury cadmium telluride; DTGS: deuterated triglycine sulfate; CF: Christiansen feature.

Authors' contributions

AM designed the study, including all the setup adaptations, and performed all the measurements. JH participated to the design of the study and to the data analysis. SF contributed to the measuring process and to data calibration and analysis. BD helped framing our results in a perspective of thermal modeling. MD'A contributed with the discussion of the results and with drafting the manuscript. All authors read and approved the final manuscript.

Authors' information

AM is a postdoc at the Institute of Planetary Research of the German Aerospace Center (DLR) in Berlin, Germany. He is co-investigator in several ESA planetary mission and part of the scientific team in NASA and JAXA missions. He is the laboratory manager of the Planetary Emissivity Laboratory (PEL). JH is leader of the Planetary Spectroscopy Laboratory group at the Institute of Planetary Research of the German Aerospace Center (DLR) in Berlin, Germany. He is Co-PI of the MERTIS instrument on BepiColombo and CoI of several instruments among them the TIR and MARA instrument on Hayabusa2. SF is a postdoc at the Institute of Planetary Research of the German Aerospace Center (DLR) in Berlin, Germany. BD is a researcher at the Department of Physics and Astronomy at Uppsala University, primarily working on thermophysical modeling for solar system small bodies. He is the Swedish Lead Scientist and Co-Investigator of the OSIRIS camera system on the ESA spacecraft Rosetta. MD'A is a postdoc at the Institute of Planetary Research of the German Aerospace Center (DLR) in Berlin, Germany.

Author details

[1] Institute of Planetary Research, German Aerospace Center DLR, Rutherfordstr. 2, 12489 Berlin, Germany. [2] Department of Physics and Astronomy, Uppsala University, Box 516, 75120 Uppsala, Sweden.

Acknowledgements

All the authors except BD are founded by the German Aerospace Center (DLR). The Planetary Emissivity Laboratory (PEL) is founded and operated by the German Aerospace Center (DLR). SF acknowledges the "Deutscher Akademischer Austausch Dienst" (DAAD) for the financial support.

Competing interests

The authors declare that they have no competing interests.

Received: 23 September 2015 Accepted: 13 June 2016
Published online: 11 July 2016

References

Baldridge AM, Hook SJ, Grove CI, Rivera G (2009) The ASTER spectral library version 2.0. Remote Sens Environ 113:711–715

Barucci MA, Fornasier S, Dotto E, Lamy PL, Jorda L, Groussin O, Brucato JL, Carvano J, Alvarez-Candal A, Cruikshank D, Fulchignoni M (2008) Asteroids 2867 Stein and 21 Lutetia: surface composition form infrared observations with the Spitzer space telescope. A&A 477:665–670

Barucci MA, Belskaya IN, Fornasier S, Fulchignoni M, Clark BE, Coradini A, Capaccioni F, Dotto E, Birlan M, Leyrat C, Sierks H, Thomas N, Vincent JB (2012) Overview of Lutetia's surface composition. Planet Space Sci 66:23–30

Biver N, Hofstadter M, Gulkis S, Bockelée-Morvan D, Choukroun M, Lellouch E, Schloerb FP, Rezac L, Ip WH, Jarchow C, Hartogh P, Lee S, von Allmen P, Crovisier J, Leyrat C, Encrenaz P (2015) Distribution of water around the nucleus of comet P/Churyumov-Gerasimenko at 3.4 AU from the Sun as seen by the MIRO instrument on Rosetta. A&A 15:1–7. doi:10.1051/0004-6361/201526094

Bland PA, Alard O, Gounelle M, and Rogers NW (2003) Trace element variation in carbonaceous chondrite matrix. In: 34th lunar and planetary science conference, Clear Lake, Texas, 17–21 March 2003, abstract 1750

Bland PA, Cressey G, Menzies ON (2004) Modal mineralogy of carbonaceous chondrites by X-ray diffraction and Mössbauer spectroscopy. Meteorit Planet Sci 39(1):3–16

Brearley AJ (1996) Nature of matrix in unequilibrated chondrites and its possible relationship to chondrules. In: Hewins RH, Jones RH, Scott ERD (eds) Chondrules and the protoplanetary disk. Cambridge University Press, Cambridge, pp 137–151

Burbine TH, Buchanan PC, Binzel RP, Bus SJ, Hiroi T, Hinrichs JL, Meibom A, Mccoy TJ (2001) Vesta, Vestoids, and the howardite, eucrite, diogenite group: relationships and the origin of spectral differences. Meteorit Planet Sci 36(6):761–781

Chabrillat S, Ben-Dor E, Viscarra Rossel RA, Demattê JAM (2013) Quantitative soil spectroscopy. Appl Environ Soil Sci 2013:1–3

Christensen PR, Bandfield JL, Hamilton VE, Howard DA, Lane MD, Piatek JL, Ruff SW, Stefanov WL (2000) A thermal emission spectral library of rock-forming mineral. J Geophys Res 105:9735–9739

Clark RN, Swayze GA, Wise R, Livo E, Hoefen T, Kokaly R, Sutley SJ (2007) USGS digital spectral library splib06a. U.S. Geological Survey, Digital Data Series, Reston

Cloutis EA, Izawa MRM, Pompilio L, Reddy V, Hiesinger H, Nathues A, Mann P, Le Corre L, Palomba E, Bell JF III (2013) Spectral reflectance properties of HED meteorites + CM2 carbonaceous chondrites: comparison to HED grain size and compositional variations and implications for the nature of low-albedo features on Asteroid 4 Vesta. Icarus 223:850–877

Davidsson BJR, Rickman H, Bandfield JL, Groussin O, Gutiérrez PJ, Wilska M, Capria MT, Emery JP, Helbert J, Jorda L, Maturilli A, Mueller TG (2015) Interpretation of thermal emission. I. The effect of roughness for spatially resolved atmosphereless bodies. Icarus 252:1–21

De Sanctis MC, Combe JPh, Ammannito E, Palomba E, Longobardo A, McCord TB, Marchi S, Capaccioni F, Capria MT, Mittlefehldt DW, Pieters CM, Sunshine J, Tosi F, Zambon F, Carraro F, Fonte S, Frigeri A, Magni G, Raymond CA, Russell CT, Turrini D (2012) Detection of widespread hydrated materials on Vesta by the VIR imaging spectrometer on board the dawn mission. Astrophys J Lett 758(2):1–5

Farmer VC (1974) The Infrared Spectra of Minerals. Mineral Soc Monogr 4:1–539

Fuchs LH, Olsen E, Jensen KJ (1973) Mineralogy, mineral-chemistry, and composition of the Murchison (C2) meteorite. Smithson Contrib Earth Sci 10:1–39

Gaffey MJ (1976) Spectral Reflectance Characteristics of the Meteorite Classes. J Geophys Res 81:905–919

Glassmeier KH, Boehnhardt H, Koschny D, Kührt E, Richter I (2007) The Rosetta mission: flying towards the origin of the solar system. Space Sci Rev 128(1–4):1–21

Grott M, Knollenberg, J, Maturilli A, Helbert J, Müller N, Kürt E (2013) Mineralogical surface characterization using the MASCOT radiometer MARA on the Hayabusa 2 mission. In: 44th lunar and planetary science conference 2013, The Woodlands, Texas, 18–22 March 2013, Abstract 1597

Hamilton VE, Christensen PR (2014) The OSIRIS-REx thermal emission spectrometer (OTES). EGU general assembly 2014, Vienna, Austria, 27 April–2 May, 2014, abstract 4687

Hasegawa S, Murakawa K, Ishiguro M, Nonaka H, Takato N, Davis CJ, Munetaka U, Hiroi T (2003) Evidence of hydrated and/or hydroxylated minerals on the surface of asteroid 4 Vesta. Geophys Res Lett 30:2123–2126

Heinemann E, Kürt E, Ulamec S (2013) Rosetta at a glance—technical data and timeline. German Aerospace Center (DLR). http://web.archive.org/web/20140108163512/http://www.dlr.de/dlr/en/desktopdefault.aspx/tabid-10395/584_read-386//usetemplate-print/

Helbert J, Maturilli A, D'Amore M (2013) Visible and near-infrared reflectance spectra of thermally processed synthetic sulfides as a potential analog for the hollow forming materials on Mercury. EPSL 369–370:233–238. doi:10.1016/j.epsl.2013.03.045

Hiroi T, Binzel RP, Sunshine JM, Pieters CM, Takeda H (1995) Grain sizes and mineral compositions of surface regoliths of vesta-like asteroids. Icarus 115:374–386

Iijima S, Buseck PR (1975) High resolution electron microscopy of enstatite I: twinning, polymorphism, and polytypism. Am Mineral 60:758–770

Iwata T, Kitazato K, Abe M, Arai T, Nakauchi Y, Nakamura T, Osawa T, Hiroi T, Matsuoka M, Matsuura S, Ozaki M, Watanabe S, and NIRS3 Team (2014) Performances of flight model of NIRS3: the near infrared spectrometer on Hayabusa-2. EPSC Abstracts 9, EPSC2014-338

King AJ, Solomon JR, Schofield PF, Russell SS (2015) Characterising the CI and CI-like carbonaceous chondrites using thermogravimetric analysis and infrared spectroscopy. Earth Planets Space 67:198. doi:10.1186/s40623-015-0370-4

Kitajima F, Uesugi M, Karouji Y, Ishibashi Y, Yada T, Naraoka H, Abe M, Fujimura A, Ito M, Yabuta H, Mita H, Takano Y, Okada T (2015) A micro-Raman and infrared study of several Hayabusa category 3 (organic) particles. Earth Planets Space. doi:10.1186/s40623-015-0182-6

Lauretta DS, Bartels AE, Barucci MA, Bierhaus EB, Binzel RP, Bottke WF, Campins H, Chesley SR, Clark BC, Clark BE, Cloutis EA, Connolly HC, Crombie MK, Delbó M, Dworkin JP, Emery JP, Glavin DP, Hamilton VE, Hergenrother CW, Johnson CL, Keller LP, Michel P, Nolan MC, Sandford SA, Scheeres DJ, Simon AA, Sutter BM, Vokrouhlický D, Walsh KJ (2015) The OSIRIS-REx target asteroid 101955 Bennu: constraints on its physical, geological, and dynamical nature from astronomical observations. Meteorit Planet Sci 50(4):834–849

Logan LM, Hunt GR (1970) Emission spectra of particulate silicates under simulated lunar conditions. J Geophys Res 75(32):6539–6548

Logan LM, Hunt GR, Salisbury JW, Balsamo SR (1973) Compositional implications of Christiansen frequency maximums for infrared remote sensing applications. J Geophys Res 78(23):4983–5003

Maturilli A, Helbert J (2014) Characterization, testing, calibration, and validation of the Berlin emissivity database. J Appl Remote Sens. doi:10.1117/1.JRS.8.084985

Maturilli A, Helbert J, Witzke A, Moroz L (2006) Emissivity measurements of analogue materials for the interpretation of data from PFS on Mars Express and MERTIS on Bepi-Colombo. PSS 54(11):1057–1064

Maturilli A, Helbert J, Moroz L (2008) The Berlin emissivity database (BED). PSS 56(3–4):420–425. Spectral library now available at http://figshare.com/articles/BED_Emissivity_Spectral_Library/1536469

Maturilli A, Helbert J, St. John JM, Head JW III, Vaughan WM, D'Amore M, Gottschalk M, Ferrari S (2014) Komatiites as Mercury surface analogues: spectral measurements at PEL. EPSL 398:58–65. doi:10.1016/j.epsl.2014.04.035

Maturilli A, Helbert J, D'Amore M, Ferrari S (2015). Experimental verification of validity for Kirchhoff's law (E = 1 − R) in vacuum and purged air. In: 46th lunar and planetary science conference 2015, The Woodlands, Texas, 16–20 March 2015, Abstract 1722

McCord TB, Sotin C (2005) Ceres: evolution and current state. J Geophys Res 110(E5):E05009:1–E05009:14

Miyamoto M (1988) Hydration bands near 3 μm and weathering of some Antarctic meteorites. EPSL 89:398–402

Morlok A, Koike C, Tomioka N, Mann I, Tomeoka K (2010) Mid-infrared spectra of the shocked Murchison CM chondrite: comparison with astronomical observations of dust in debris disks. Icarus 207(1):45–53

Morlok A, Koike C, Tomeoka K, Mason A, Lisse C, Anand M, Grady M (2012) Mid-infrared spectra of differentiated meteorites (achondrites): comparison with astronomical observations of dust in protoplanetary and debris disks. Icarus 219:48–56

Moroz LV, Schmidt M, Schade U, Hiroi T, Ivanova MA (2006) Synchrotron-based infrared microspectroscopy as a useful tool to study hydration states of meteorite constituents. Meteorit Planet Sci 41(8):1219–1230

Mueller T, Durech J, Hasegawa S et al (2010) Thermo-physical properties of 162173 (1999 JU3), a potential flyby and rendezvous target for interplanetary missions. A&A. doi:10.1051/0004-6361/201015599

Mustard JF, Hays JE (1997) Effects on hyperfine particles on reflectance spectra from 0.3 to 25 μm. Icarus 125:145–163

Nakamura T, Noguchi T, Tanaka M, Zolensky Kimura M, Tsuchiyama A, Nakato A, Ogami T, Ishida H, Uesugi M, Yada T, Shirai K, Fujimura A, Okazaki R, Sandford SA, Ishibashi Y, Abe M, Okada T, Ueno M, Mukai T, Yoshikawa M, Kawaguchi J (2011) Itokawa dust particles: a direct link between S-type asteroids and ordinary chondrites. Science 333(1113):1116

Okada T, Fukuhara T, Tanaka S, Taguchi M, Nakamura R, Sekiguchi T, Hasegawa S, Ogawa Y, Kitazato K, Matsunaga T, Imamura T, Wada T, Arai T, Yamamoto Y, Takaki R, Tachikawa S, Helbert J, Mueller T, and Hayabusa2 Thermal-Infrared Imager (TIR) Team (2012) Thermal infrared imager TIR on Hayabusa2 to investigate physical properties of C-class near-earth asteroid 1999JU3. In: 43th lunar and planetary science conference 2012, The Woodlands, Texas, 19–23 March 2012, Abstract 1498

Pieters CM, Fischer EM, Rode O, Basu A (1993) Optical effects of space weathering: the role of the finest fraction. J Geophys Res 98(E11):20817–20824

Rivkin AS, McFadden LA, Binzel RP, Sykes M (2006) Rotationally-resolved spectroscopy of Vesta I: 2–4 μm region. Icarus 180(2):464–472

Rivkin AS, Li JY, Milliken RE, Lim LF, Lovell AJ, Schmidt BE, McFadden LA, Cohen BA (2011) The surface composition of ceres. Space Sci Rev 163(1–4):95–116

Rubin AE (1997) Igneous graphite in enstatite chondrites. Mineral Mag 61:699–703

Russell CT, Capaccioni F, Coradini A, De Sanctis MC, Feldman WC, Jaumann R, Keller HU, McCord TB, McFadden LA, Mottola S, Pieters CM, Prettyman TH, Raymond CA, Sykes MV, Smith DE, Zuber MT (2007) Dawn mission to Vesta and Ceres. Earth Moon Planets 101:65–91

Saiki T, Sawada H, Okamoto C, Yano H, Takagi Y, Akahoshi Y, Yoshikawa M (2013) Small carry-on impactor of Hayabusa2 mission. Acta Astronaut 84:227–236

Salisbury JW, Hunt GR (1974) Meteorite spectra and weathering. JGR 79:4439–4441

Salisbury JW, Walter LS (1989) Thermal infrared (2.5 to 13.5 μm) spectroscopic remote sensing of igneous rocks types on particulate planetary surfaces. JGR 94:9192–9202

Salisbury JW, D'Aria DM, Jarosewich E (1991) Midinfrared (2.5-13.5 μm) reflectance spectra of powdered stony meteorites. Icarus 92:280–297

Salisbury JW, Wald A, D'Aria DM (1994) Thermal-infrared remote sensing and Kirchhoff's law 1. Laboratory measurements. JGR 99(B6):11897–11911

Scott ERD, Barber DJ, Alexander CM, Hutchison R, Peck JA (1988) Primitive material surviving in chondrites: matrix. In: Kerridge JF, Matthews MS (eds) Meteorites and early solar system. University of Arizona Press, Tucson, pp 718–745

Simon-Miller AA, and Reuter DC (2013) OSIRIS-REx OVIRS: A Scalable Visible to Near-IR Spectrometer for Planetary Study. 44th lunar and planetary science conference 2013, The Woodlands, Texas, 18–22 March 2013, Abstract 1100

Tsuchiyama A, Uesugi M, Matsushima T, Michikami T, Kadono T, Nakamura T, Uesugi K, Nakano T, Sandford SA, Noguchi R, Matsumoto T, Matsuno J, Nagano T, Imai Y, Takeuchi A, Suzuki Y, Ogami T, Katagiri J, Ebihara M, Ireland TR, Kitajima F, Nagao K, Naraoka H, Noguchi T, Okazaki R, Yurimoto H, Zolensky ME, Mukai T, Abe M, Yada T, Fujimura A, Yoshikawa M, Kawaguchi J (2011) Three-dimensional structure of Hayabusa samples: origin and evolution of Itokawa Regolith. Science 333:1125–1128

Uesugi M, Naraoka H, Ito M, Yabuta H, Kitajima F, Takano Y, Mita H, Ohnishi I, Kebukawa Y, Yada T, Karouji Y, Ishibashi Y, Okada T, Abe M (2014) Sequential analysis of carbonaceous materials in Hayabusa-returned

samples for the determination of their origin. Earth Planets Space 66:102. doi:10.1186/1880-5981-66-102
Vernazza P, Lamy P, Groussin O, Hiroi T, Jorda L, King PL, Izawa MRM, Marchis F, Birlan M, Brunetto R (2011) Asteroid (21) Lutetia as a remnant of Earth's precursor planetesimals. Icarus 216:650–659
Vilas F, Gaffey MJ (1989) Phyllosilicate absorption features in main-belt and outer-belt asteroid reflectance spectra. Science 246:790–792
Zellner B, Leake M, Morrison D, Williams JG (1977) The E asteroids and the origin of the enstatite achondrites. Geochim Cosmochim Acta 41(12):1759–1767